Research article

Yan Liu, Soo-Jin Chua*, Siping Gao, Wenrui Hu and Yongxin Guo

Electroluminescence in plasmonic actuator based on Au/SiO_2/n-Si tunnel junction

https://doi.org/10.1515/nanoph-2021-0287
Received June 7, 2021; accepted August 20, 2021;
published online September 3, 2021

Abstract: A compact electrical source capable of generating surface plasmon polaritons would represent a crucial step for on-chip plasmonic circuitry. The device fabrication of plasmonic actuator based on Au/SiO_2/n^{++}Si tunnel junction and performance have been reported in [ACS photonics, 2021, 8, 7, 1951–1960]. This work focuses on the underlying mechanisms of electroluminescence. The n-type Si samples were doped with concentrations ranging from 1.6×10^{15} cm^{-3} to 1.0×10^{20} cm^{-3}. A low voltage of 1.4 V for intense light emission was achieved at the highest concentration. The electrical/spectral characteristics and energy band diagrams calculation show two distinct behaviors indicating two distinct mechanisms of light emission are at work in the heavily doped versus the lightly doped Si. In the heavily doped case, the light output is correlated to tunneling current and the subsequent conversion of surface plasmons to photons, while that for the lightly doped case is due to indirect band-to-band recombination in silicon. The results are validated by numerical simulation which indicates that the heavy doping of the n^{++}-Si is necessary to achieve surface plasmon generation via electron tunneling due to the presence of band tail states and their effect on lowering the barrier height.

Keywords: band tail states; doping concentration; phonon-assisted indirect radiative recombination; plasmonic actuator; surface-plasmon assisted emission.

***Corresponding author: Soo-Jin Chua**, Department of Electrical and Computer Engineering, 4 Engineering Drive 3, National University of Singapore, Singapore 117576, Singapore; and LEES Program, Singapore-MIT Alliance for Research & Technology (SMART), Singapore 138602, Singapore, E-mail: elecsj@nus.edu.sg
Yan Liu, Siping Gao, Wenrui Hu and Yongxin Guo, Department of Electrical and Computer Engineering, 4 Engineering Drive 3, National University of Singapore, Singapore 117576, Singapore. https://orcid.org/0000-0003-4969-1888 (Y. Liu)

1 Introduction

The past two decades has seen an unprecedented increase in the amount of digital information transmitted all over the world. The rapid growth of computing power and the data transmission speed have changed our way of life and work. An important invention in the information age, the complementary metal-oxide semiconductor (CMOS), is now approaching its fundamental limit on its feature size and interconnect dimension hindering further progress in device integration predicted by Moore's law. Integration of electronics with photonics is one way forward to achieve more than Moore's. Plasmonic, as an integration of electronic and photonic device, is considered a very promising technology platform for the development of next generation of chip in the more than Moore's era [1]. Plasmonic devices are the building blocks for a new generation of ultrafast and ultracompact nanophotonics chip, including active components (plasmonic actuator [2–4]), plasmonic detector [5], plasmonic modulator [6]) and passive components (plasmonic waveguide [7]). Among these, the plasmonic actuator is one of the most important components in plasmonic circuits serving as the plasmon source interfacing between electronics and photonics. Recent achievements have resulted in the surface plasmon polaritons (SPP) excitation efficiency in metal–insulator–metal (MIM) tunnel junction(TJ) exceeding 1% as reported by W. Du et al. and H. L. Qian et al. [2, 3] and in modulating the emission spectrum as demonstrated by X. B. He [4].

As an active component, the silicon-based plasmonic actuator consisting of a metal–insulator–silicon (MIS) tunnel junction can fulfill the role of current-plasmon conversion and be integrated in Si integrated circuit (IC) mass production. The plasmonic waveguide consisting of metal lines embedded in dielectric films in back-end of line in CMOS technology are suitable for SPPs transmission [8]. Therefore, both active and passive plasmonic components integrated on a silicon chip have received significant attention recently [9]. A silicon-based plasmonic device using SPPs for signal transmission working at optical frequencies has the advantage of small feature size not limited by the diffraction limit of light. The first observation of

surface plasmon excitation in degenerate semiconductor [10] by tunneling electrons was traced back to 1969. In 1993, J. Watanabe et al. [11] observed visible light from Si–metal–oxide–semiconductor tunnel junction due to SPP excitation. They claimed that the tunneling current radiated light by scattering from residual surface roughness. A similar piece of work was reported by M. X. Wang in 2000 [12] who applied a very large DC voltage bias (5–7 V) on MIS tunnel junctions to generate surface plasmon and observed light emission. In 2018, H. Goktas [13] observed light emission from a p-type silicon doped with 2×10^{17} cm^{-3} and proposed that the emission is due to tunneling of accumulated holes generating a combination of hybrid-photon–plasmon mode and a surface plasmon mode. However, the reports mentioned earlier do not have enough data to conclusively deduce that the light generation is due to plasmon–photon outcoupling. For practical application in nanophotonics, there is a need to generate and read out the plasmonic signals by electrical means only [2], without involving any intermediate generation of excitons or photons. Thus, any forms of intermediate process such as generation of hybrid plasmon–photon modes may reduce efficiency of plasmonic devices and increase transmission loss. Here we propose the model for an electrically driven SPP in an Au/SiO_2/n^{++}Si tunnel junction which showed plasmon excitation at a low voltage of 1.4 V. The device fabrication of the Au/SiO_2/n^{++}Si tunnel junctions and performance have been reported in [ACS photonics, 2021, **8**, 7, 1951–1960]. This work focuses on the theoretical analysis of the electroluminescence in Au/SiO_2/n^{++}Si junctions with different doping concentrations. The C–V behaviors of metal–insulator–Si (MIS) TJs with different levels of doping concentrations have been presented to help interpret the capacitance contributed by band tail states and highlight the crucial role they play in the electron tunneling process. The computed energy diagrams have been provided to explain the underlying mechanism of electroluminescence in MIS TJ with different levels of doping concentrations. We have also included the simulation of the electroluminescence spectra as a function of applied voltage for different doped samples to compare with the experimental results reported in the earlier ACS photonics paper.

2 Device design and characterizations

A desirable option is to use purely quantum tunneling of electrons across an electrically biased barrier between the n-type silicon and a metal contact (Au) to excite surface plasmon at the gold/dielectric interface. In the process of electron transmission to the metal from silicon, the electrons can either (1) tunnel elastically without any energy loss, or (2) tunnel inelastically imparting the energy to the free electrons in the gold electrode and generating surface plasmons [14], or (3) overshoot the barrier under a high voltage bias i.e. via thermionic emission [15]. Here, we report on the demonstration of an electrically driven, Au/SiO_2/n-Si plasmonic actuator based on the inelastic electron tunneling process at room temperature and study the mechanism of light emission from metal–oxide–silicon junctions with n-type doping concentrations varying by four orders of magnitude in silicon substrates. Figure 1a shows the perspective view of the Au/SiO_2/n-Si junction, consisting of a heavily doped n-type silicon substrate with a thermally grown SiO_2 (th-SiO_2) layer of ~2 nm as a tunneling barrier, a 40-nm-thick gold film on the top of junction area, and a 200-nm-thick gold as a top electrode outside of cross-point junction, as demonstrated in our previous work [16]. The 100-nm-thick oxide layer formed by sputtering (sp-SiO_2) covers an area wider than the junction area of ~5×5 μm to ensure that the current detected is obtained via tunneling through the 2 nm SiO_2 barrier. The top view of Au/SiO_2/n-Si junction was shown in Figure 1b. To facilitate electrical and optical measurements, the whole silicon chip comprising of an array of 6×6 tunnel junctions is housed in a ceramic butterfly package with wires bonded for electrical contact. This large number of samples is to ensure the reproducibility of the events observed. Here, the forward current is defined corresponding to majority carriers (electrons) flow from semiconductor to metal, while the reverse current flow is from metal to semiconductor. It is found that the forward current flow is strongly correlated with doping concentration of n-type Si. In the case of heavy doping in n^{++}-Si, the forward electron current flow from n^{++}-Si to Au is dominated by quantum tunneling, accompanied by surface plasmons excitation, as shown in Figure 1c. In the case of lightly doped n-Si (as shown in Figure 1d), the small amount of electron current flow is mainly contributed by majority carriers (electrons) in n-Si tunneling with a low probability through a thin SiO_2 barrier to Au, when a large positive voltage (>5 V) is applied on the Au electrode. Meanwhile, a large quantity of electrons accumulates at the n-Si/SiO_2 interface resulting in electron–hole recombination in Si via indirect band-to-band transition assisted by phonons. This inefficient recombination process results in few photons being emitted. The heavily doped n^{++}-Si is employed to ensure sufficient band tail states in the band gap of n^{++}-Si to aid the tunneling process through lowering of the oxide barrier. In this work, a positive DC bias, V_b is applied on the gold electrode of the Au/SiO_2/n^{++}-Si tunnel junction to inject electrons into the

metal and voiding any photons generation by electron–hole indirect phonon-assisted recombination in the silicon. The calculated band diagram for this situation is shown in Figure 1e. In quantum tunneling, an electron with a wave function of $\psi_{Si}(E)$ in the conduction band ($E_{fs} \geq E_c$) with energy of E ($\geq E_{fs} - E_{fAu}$) tunneling through the SiO_2 barrier to the gold contact under the positive voltage may result in two possible pathways: (1) elastic tunneling without any energy loss, arriving at the gold contact with the wave function of $\psi_{Au}(E)$. (2) inelastic tunneling losing an energy of $\hbar\omega$

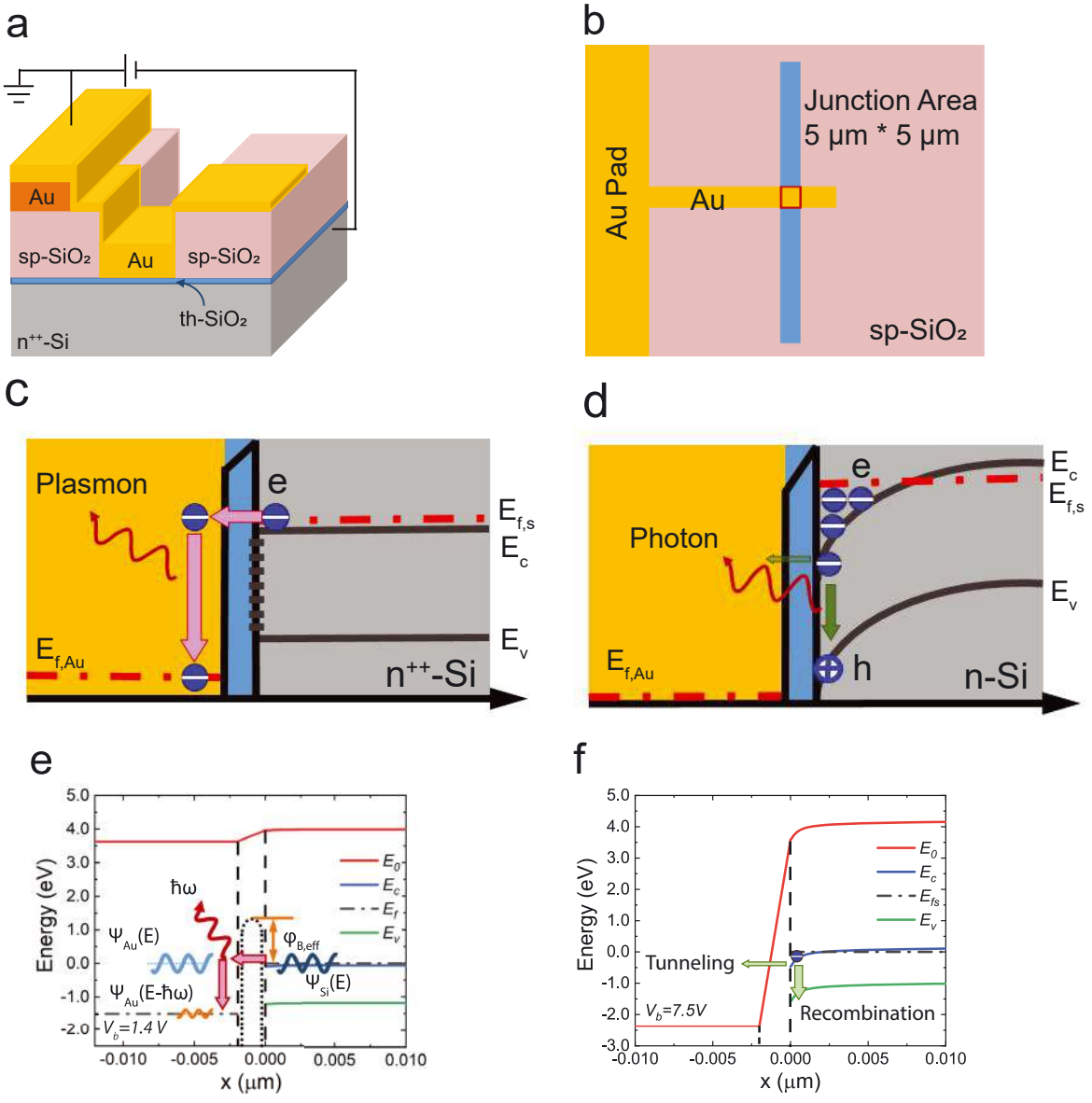

Figure 1: (a) Schematic of Au/SiO_2/n-Si tunnel junction consisting of gold strip electrode (thickness 40 nm and width 5 μm) on the n^{++}-Si substrate (thickness ~ 500 μm) within a 2-nm-thick thermal SiO_2 ("th-SiO_2") in between. Au/SiO_2/n-Si plasmons are excited in junction area. "sp-SiO_2" stands for sputtered oxide. (b) The top view of MIS tunnel junction (in red frame) with an area of 5 × 5 μm. (c) A schematic of energy diagram at low forward bias of Au/SiO_2/n^{++}-Si showing quantum tunneling mechanism dominating the forward current flow and plasmons generation originating from inelastic tunneling. The short horizontal black lines at n^{++}-Si/SiO_2 interface stand for band tail states in the silicon band gap. (d) A schematic of Au/SiO_2/n-Si to show the mechanism of light emission caused by electron–hole recombination in silicon when a large positive voltage is applied on Au. (e) Calculated energy band diagram of the MIS tunnel junction with a positive voltage bias $V_b = 1.4$ V on top electrode Au for case of n^{++}Si. The red arrow indicates an inelastic electron tunneling process resulting in surface plasmon excitation with the energy of $\hbar\omega$ (wiggly arrow). The tunneling barrier height is $\varphi_{B,eff}$. (f). Calculated energy band diagram of MIS junction with a large positive voltage bias $V_b = 7.5$ V on top electrode Au. A thin green horizontal arrow represents a small number of electrons tunneling through SiO_2 barrier, and the thick green arrow indicates the accumulated electrons at conduction band at the n-Si/SiO_2 interface recombining with the holes at the valence band.

($eV_b \geq \hbar\omega$), arriving at gold contact with a wave function of $\psi_{Au}(E - \hbar\omega)$, where $\hbar$ is the reduced Planck constant and ω is the angular frequency of the optical mode. In the inelastic tunneling pathway (2), the tunneling electrons may impart the energy ($\hbar\omega$) to the free electrons in the gold film, resulting in free electrons oscillation, and generating a surface plasmon mode at the Au/SiO_2 interface. The light emission originates from the surface plasmon mode out-coupling via a very thin and narrow Au strip with rough edges. The 100-nm-thick oxide layer formed by sputtering (sp-SiO_2) covers an area wider than the junction area of ~5 × 5 μm to ensure that the current detected is obtained via tunneling through the 2 nm SiO_2 barrier. In the calculated energy band diagram of Figure 1f, with a low doped n-Si, a very large positive voltage bias (V_b = 7.5 V) is needed to be applied on the Au contact to achieve a faint light emission, resulting in the majority carriers (electrons) in conduction band accumulating at n-Si/SiO_2 interface. Some of electrons tunnel through with a very low tunneling probability due to a triangle shape SiO_2 barrier height of ~4.25 eV.

To prove that a surface plasmon mode is indeed excited, the *I*–*V* characteristics of four types of MIS junctions with different n-doping concentrations (1.0×10^{20} cm^{-3}, 3.6×10^{18} cm^{-3}, 1.9×10^{16} cm^{-3}, and 1.6×10^{15} cm^{-3}) were measured. By applying a positive DC bias (positive voltage on the Au electrode as shown in Figure 1a) across the MIS junction, electrons tunnel through the oxide barrier. Simultaneously, the light emitted from the junction is captured by an inverted microscope for spectral analysis [2]. The intensity of the light output is determined by the external quantum efficiency (η_{MIS}) comprising of the product of internal quantum efficiency (conversion of electrons to plasmons) and the radiation efficiency (conversion of plasmons to photons). Generally, the internal quantum efficiency is strongly correlated to the probability of inelastic tunneling events [17]. With heavy doping concentration in n^{++}-Si, more electrons are available to participate in the tunneling process because of a large concentration of band tail states of n^{++}-Si. At the same time, these charged band tail states at the n^{++}-Si/SiO_2 interface act to lower the barrier height through image force bearing in mind that the oxide layer is only 2 nm thick. The rough edges of the tunnel junction may provide a spectrum of k-vectors to facilitate the conversion of surface plasmons to photons. The radiation efficiency improvement has been investigated by K. S. Makarenko et al., and it shows that the roughness of electrode is very important for surface plasmon out coupling into photons [18]. Previous work has shown that quantum efficiency is prohibitively low (10^{-4}–10^{-7}) [19–23]. Therefore, improving quantum efficiency in plasmonic device is fundamental to engineering an efficient plasmonic actuator.

3 Results and discussions

The underlying physical mechanism of surface plasmon mode excitation is based on quantum-mechanical inelastic electron tunneling across a barrier. To identify the effect of the density of free carriers on tunneling MIS junctions, on the magnitude of the tunneling current, four different doping concentrations (N_d) in n-type Si substrates are used viz. 1.0×10^{20} cm^{-3}, 3.6×10^{18} cm^{-3}, 1.9×10^{16} cm^{-3}, and 1.6×10^{15} cm^{-3}. The fabrication process of the MIS junction is reported in our previous work [16]. *I*–*V* and *C*–*V* characterization of Au/SiO_2/n-Si junctions were performed using a Keithley 4200A-SCS semiconductor parameters analyzer with multichannel automatic switching modules. Four chips, each with a different doping level, are packaged for the characterization. Each chip is comprised of an array of 6 × 6 junctions. Figure 2a shows the typical *I*–*V* characteristics over the voltage range from −2 to 2 V, of four MIS junctions with different orders of magnitude in doping concentrations. The *I*–*V* curve for each doping concentration is very repeatable among the 6 × 6 array of devices in each chip. The approximate symmetry of the *I*–*V* curves for positive and negative bias voltages of the two samples with $N_d = 1.0 \times 10^{20}$ cm^{-3} and 3.6×10^{18} cm^{-3} indicates that the free electrons tunneling occurs through the 2-nm SiO_2 barrier in both directions with the same ease. In comparison, the asymmetry of the *I*–*V* curves with respect to voltages of samples with $N_d = 1.9 \times 10^{16}$ cm^{-3} and 1.6×10^{15} cm^{-3} implies that the accumulation layer and the Schottky barrier mediate differently the electrical conduction path in the positive and negative bias, respectively. Dahlke [24, 25] had investigated an MIS TJ formed by dry oxidation of Si and showed that it has a high density of band tail states. In heavily doped n^{++}-Si, there is a narrowing of bandgap due to band tails. Thus, it appears that band tail states and the narrowing of bandgaps make the *I*–*V* curves of an MIS tunnel structure more like those of an MIM tunnel structures. The high density of band tail states at the SiO_2/n^{++}-Si aids the electrons tunneling from the n^{++}-Si into the conduction band of gold. Here, the band tails smear out the effect of the energy band gap of silicon, giving credence to the use of MIM tunneling theory to analyze MIS tunnel structures with Si heavily doped. In this work, quantum tunneling theory was used to estimate the Au-SiO_2 ($\varphi_{B,eff}$) barrier height in an MIS tunnel junction with degenerate n-type silicon [26] (Figure S1(a) and (b)). It must be noted that the abundance of band tail states at the SiO_2/Au and at SiO_2/n^{++}-Si coupled with the small width of the oxide layer results in the lowering (by image force) of the actual barrier height in the oxide to the effective barrier height, $\varphi_{B,eff}$. By extracting the tunneling barrier ($\varphi_{B,eff}$) in

the tunnel MIS junctions, it is found that the higher doping concentration of $N_d = 1.0 \times 10^{20}$ cm^{-3} lowers the tunneling barrier height to $\varphi_{B,eff} = 1.69$ eV from the theoretical value of 4.25 eV. This lower barrier height results in a larger tunneling current flow at the positive voltage bias. It is therefore expected that the surface plasmon mode would be excited at a lower electrical bias in highly doped MIS tunnel junction. In the other group of MIS junctions with much lower doping concentrations of $N_d = 1.9 \times 10^{16}$ cm^{-3} and 1.6×10^{15} cm^{-3}, the asymmetrical I–V curves with respect to the voltage indicate that the forward current flow is dominated by a low probability tunneling due to SiO_2 barrier, whereas the reverse current flow is even lower because of a thicker barrier width comprising of SiO_2 layer and Schottky barrier. At 2 V bias, this tunneling current is two orders of magnitudes lower than that in heavily doped samples. At a very high voltage bias ($V_b \geq 5.5$ V), the accumulated electrons at the conduction band of n-Si recombine with the holes in valence band electrons. This is an indirect radiative recombination in n-Si contributing to the light emission of MIS junctions, as shown in Figure 1d and f. The lower doped n-Si does not have the charged band tail states to lower the barrier height in positive bias and thus impede the electron tunneling from n-Si to Au, resulting in a reduced forward current. More details of electrical characteristics are shown in Supplementary Note 1.

The quantum-mechanical electrons tunneling in MIS junctions should also be verified by electrical AC measurements [27]. Four capacitances are involved, C_{ox}, C_{BT}, C_{Dep}, and C_{Acm} and they are, respectively, the oxide capacitance, capacitance due to band tail states, capacitance to the depletion layer, and the capacitance due to the accumulation layer on the Si surface. The band tail states capacitance and that at the Si interface (due to either the accumulation layer or the depletion layer) are connected in parallel. The effective capacitances are then connected in series with the oxide capacitance. The C–V characteristics of the four MIS junctions with different doping concentrations were measured in the frequency range of 10–100 kHz. We now focus on 10 kHz and explain the low frequency behavior of the C–V characteristics in Figure 2b of the MIS junctions measured with the voltage bias sweeping from –2 to 2 V at an AC drive signal of 20 mV. To minimize measurement error, a larger device area of 500 × 500 μm^2 was used for the four types of MIS junctions (n-type Si: 1.0×10^{20} cm^{-3}, 3.6×10^{18} cm^{-3}, 1.9×10^{16} cm^{-3}, and 1.6×10^{15} cm^{-3}). The equivalent capacitances at positive voltage bias (C_{eq+}) (Eq. (1)) and negative voltage bias (C_{eq-}) (Eq. (2)) in MIS junctions can be expressed, respectively, as follows,

$$C_{eq+} = \frac{(C_{BT} + C_{ACM}) \times C_{ox}}{C_{BT} + C_{ACM} + C_{ox}} \quad (1)$$

$$C_{eq-} = \frac{(C'_{BT} + C_{DEP}) \times C_{ox}}{C_{BT'} + C_{DEP} + C_{ox}} \quad (2)$$

where C_{BT} is the capacitance contributed by band tail states when they are fully occupied by electrons at the interface of SiO_2/n^{++}-Si under a positive voltage bias, C'_{BT} is the capacitance contributed by the band tail states when they are partially occupied by electrons under a negative voltage bias, and both capacitances are only present in the heavily doped n^{++}-Si. The other capacitances which exist in both the heavily and low doped samples are, viz. C_{ox}, contributed by the 2-nm SiO_2 capacitance (~1.73×10^{-2} pF/μm^2); C_{ACM}, contributed by the electrons in the accumulation layer at the n-Si surface under a positive voltage bias, and C_{DEP}, the depletion layer capacitance in the n-Si region

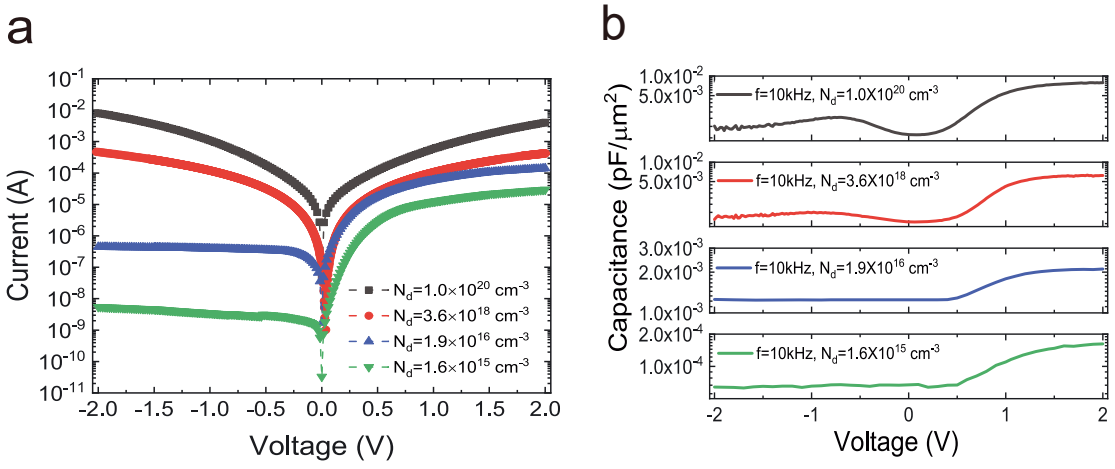

Figure 2: Electrical characteristics of MIS junctions in four doping levels in n-Si. (a) I–V curves of MIS junctions with the area of 5 × 5 μm^2, (b) C–V curves of MIS junctions with the area of 500 × 500 μm^2 at a low frequency of 10 kHz.

under a negative voltage bias. The highly doped MIS junction ($N_d = 1.0 \times 10^{20}$ cm^{-3}) is measured to have a higher capacitance (7.89×10^{-3} pF/μm^2) compared to that of the lower doped level of $N_d = 3.6 \times 10^{18}$ cm^{-3} at 2 V bias (6.20×10^{-3} pF/μm^2), as shown in Figure 2b. This is in agreement with the higher density of band tail states of 2.78×10^{12} cm^{-2} eV^{-1} for the highly doped sample compared to 1.76×10^{11} cm^{-2} eV^{-1} for the less heavily doped sample extracted from AC measurements [28]. This also applies for the measurements conducted at −2 V (The equivalent capacitances are summarized in the Supplementary Note Table S1). The equivalent circuit of Au/SiO_2/n^{++}-Si capacitance is demonstrated in Figure S2(a). So, the sum of the two capacitances (~7.89×10^{-3} pF/μm^2), i.e. band tail capacitance (C_{BT}) and accumulation capacitance C_{ACM} dominate at 2 V bias. Thus, ($C_{BT} + C_{ACM}$) is smaller than C_{ox}, in Eq. (1). And at −2 V bias, ($C_{BT'} + C_{DEP}$) is even smaller than C_{ox} in Eq. (2)). C_{BT} is larger than C'_{BT} due to the higher charge occupancy. The capacitance contributed by band tail states play a crucial role in electron tunneling process. In the lightly doped MIS junctions with the concentrations of 1.9×10^{16} cm^{-3} and 1.6×10^{15} cm^{-3}, there are no band tail capacitances ($C_{BT} = 0$). The equivalent circuit of Au/SiO_2/n-Si capacitance is demonstrated in Figure S2(b). Under negative bias (negative voltage on the Au), the equivalent capacitance (C_{eq-}) varies slightly because the capacitance is determined by a large width of depletion layer ($C_{ox} > C_{DEP}$ in Eq. (2)). Under positive voltage bias, the equivalent capacitance (C_{eq+}) increases with bias because the total charge of accumulated electron (C_{ACM}) increases ($C_{eq+} = \frac{C_{ACM} \times C_{ox}}{C_{ACM} + C_{ox}}$ in Eq. (1)), as shown in Figure 2b. The equivalent capacitance in heavily doped MIS tunnel junction is approximately 50 times larger than that in lightly doped MIS junction at 2 V bias. The largest equivalent capacitance means the smallest impedance. From the above discussion, it is seen that the band tail states formed in heavily doped MIS junction facilitates for electrons tunneling. A higher doping level, besides generating a larger concentration of free electrons, also creates band tail states which lower the tunneling barrier height. Experimental evidence of the lowering of the tunneling barrier with increase in doping concentration is provided in Supplementary Note 1. The measured values $\varphi_{B,eff}$ decreases with the heavy doping concentration.

The relationship between the electrical characteristics and optical characteristics in MIS tunnel junction has been a matter of continuous research for half a century [29]. In this work, the electroluminescence (EL) of MIS junctions with different doping concentrations was investigated under positive voltage bias. To interpret the experimental results, an FEM model is provided to explain the spectral characteristics with respect to voltage bias as a function of doping concentration (Supplementary Note 2). Experimentally, the optical images of the emission region of the MIS junctions were captured by an inverted optical microscope (Nikon Eclipse Ti-*E*) equipped with a spectrometer (Shamrock 303i) and an electron multiplying CCD (EMCCD, iXon Ultra 897). The recorded spectra of plasmon–photon conversion show the same blueshift characteristics as reported in our previous work in [2]. To increase the numerical objective, an oil immersion objective was used (NA = 1.49). The images of light emission regions (Figure 3a insets) are captured by an EMCCD with 2 min integration time and an EM gain of 300. To eliminate the emission due to interband transition in gold film, the voltage bias, V_b, is limited to below 2.4 V [30]. Here, we only discuss the results of positive biases on the MIS TJs to excite SPP on Au film. Negative biases did not result in light emission as the electrons tunneling into the n^{++}-Si is ineffective to excite bulk plasmons due to the large thickness of the substrate. The spectra are recorded for samples with different doping concentrations viz. (a) 1.0×10^{20} cm^{-3}, (b) 3.6×10^{18} cm^{-3}, and (c) 1.9×10^{16} cm^{-3} in our previous work [16]. The spectra of sample (a) show a voltage dependent peak blueshifts (voltages ranging from 1.4 to 1.9 V in Figure 3b) like the spectra reported by W. Du [2]. There is an insignificant spectral peak blueshifts (voltages ranging from 1.5 to 2.5 V) in sample (b), while no peak blueshifts are observed in sample (c). The light emission from the sample (d) with the lowest concentration of 1.6×10^{15} cm^{-3} was very weak and cannot be captured reliably by the instrument.

For an MIS tunnel junction with the highest doping concentration of $N_d = 1.0 \times 10^{20}$ cm^{-3}, the round dots in Figure 3a give the shortest wavelength or cut-off wavelength ($\lambda_{cut\text{-}off}$) in nm of the emission (corresponding to the highest photon energy). The square dots give the corresponding cut-off energy in eV. The cut-off energy of the light emission spectrum in an Au/SiO_2/n^{++}-Si tunnel junction increases linearly with the voltage bias [16]. Here we have provided the additional information of light emission intensity in six insets as well and illustrated the electroluminescence intensity increases with the voltage bias intuitively. The main features in Figure 3a and b are: with increase in voltage (1) the cut-off wavelength ($\lambda_{cut\text{-}off}$) decreases from 885.7 nm ($V_b = 1.4$ V) to 652.6 nm ($V_b = 1.9$ V), (2) the intensity of light emission at each voltage bias increases from 6.14 a.u ($V_b = 1.4$ V) to 262.40 a.u ($V_b = 1.9$ V) ,and (3) the peak of the spectrum blue shifts from 985.5 nm ($V_b = 1.4$ V) to 883.4 nm ($V_b = 1.9$ V). Feature (1) is an expression of the conservation of energy i.e. the plasmon energy ($\hbar\omega$) is less than or equal to the electron excitation energy (eV_b), while feature (2) indicates that the higher plasmon intensity is obtained at a

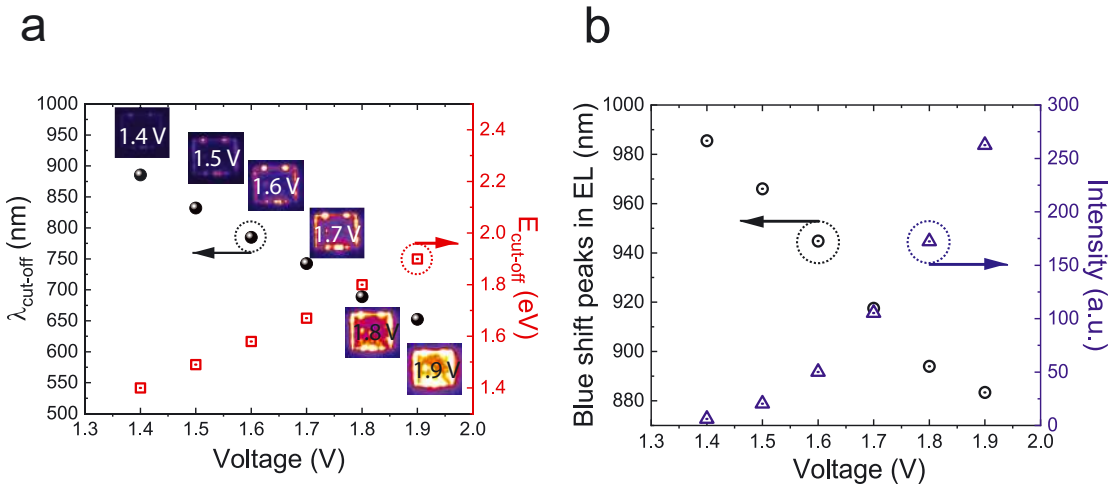

Figure 3: (a) Identification of surface plasmons conversion to photon as observed in electroluminescence experiment of the MIS tunnel junction with the highest doping concentration of 1.0×10^{20} cm^{-3}. The insets show the EMCCD images in real plane corresponding to different voltage bias (V_b) [16]. $\lambda_{cut\text{-}off}$ is the shortest wavelength emitted. (b) The peaks of spectrum blueshift from 985.5 to 883.4 nm, while the intensities of the peaks increase from 6.14 to 262.40 (a.u) with the voltage bias increasing from 1.4 to 1.9 V.

higher tunneling current corresponding to a higher voltage bias. The blue shift in the emission spectrum seen in feature (3) with increasing bias is an important feature of surface plasmon excitation which will be explained in the theoretical model to be presented later. From the six EMCCD images shown in the insets of Figure 3a, the emission from the surface of the Au film is relatively weak with high intensities distributed at the edges of the junction area in the lower voltage range from 1.4 to 1.7 V. This is due to the higher photon out-coupling from the localized surface plasmons via the rough edges of the Au strip [31]. At 1.9 V, the whole junction area is lighted up brightly due to the surface plasmon outcoupling through the 40-nm thin Au film as well [18]. It is worthy to note that at the highest doping concentration of 1.0×10^{20} cm^{-3}, plasmons can be excited at a low voltage bias of 1.4 V in the MIS tunnel junction, which is much lower than the higher voltage bias ranging from 2 to 8 V reported by other groups [12, 13, 32–41].

Figure 4a and b shows the plots of the η_{MIS}, defined as the quantity of emitted surface plasmon polaritons per tunneling electron and per unit spectral width (Supplementary Note 2), which correspond to samples (a) and (b). At a given bias, η_{MIS} is proportional to the plasmon intensity and in turn gives rise to the light intensity assuming the out-coupling efficiency is independent of wavelength. The method of calculating η_{MIS} is as per reference [42] but by replacing the MIM junction with an MIS junction. This requires changing the optical parameters such as refractive indices of the metal with that of the n-type Si which is doping concentration dependent. It is seen that the simulated results of the spectra at different bias match the experimental results qualitatively. The detail of the simulation is shown in Supplementary Note 2. They show the same features as described earlier viz. the peak wavelength blue shifts with bias for the heavily doped sample while the low doped sample has a constant peak wavelength corresponding to the bandgap energy. For the lightly doped MIS junction (Sample (c)), the light emission is based on phonon-assisted indirect radiative recombination in n-Si. Hence, the normalized electroluminescence efficiency of

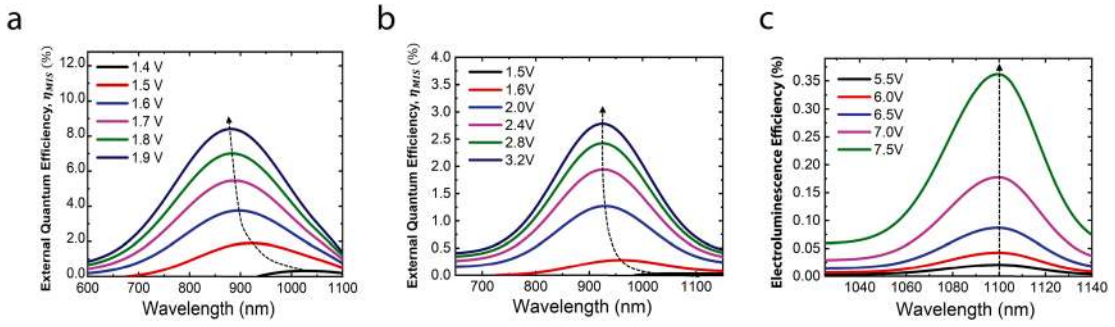

Figure 4: The external quantum efficiency, η_{MIS}, of (a) $N_d = 1.0 \times 10^{20}$ cm^{-3}, (b) $N_d = 3.6 \times 10^{18}$ cm^{-3} and the electroluminescence efficiency of (c) $N_d = 1.9 \times 10^{16}$ cm^{-3} from FEM models. η_{MIS} can be interpreted to be proportional to the emitted photon flux.

MIS junction with a doping concentration of 1.9×10^{16} cm^{-3} is calculated by FEM model as shown in Figure 4c.

To analyze the mechanisms of electrical conduction and the phenomenon of light emission in the MIS junctions, the energy band diagram calculations (TCAD_Sentaurus_2014.09-SP1) for Au/SiO_2/n-Si structures are indispensable. Figure 5a–d shows the simulation results of the energy band (with energy levels E_0, E_c, E_f, E_v) in Au/SiO_2/n-Si structure under zero and positive bias. To understand the blueshift in the spectra with voltage bias, in the samples with high doping concentrations, the band diagrams shown in Figure 5a and b are used. It is seen in both Figure 5a and b that the emission energy ($E_{cut\text{-}off}$) increases with bias as indicated by the longer vertical blue arrows with solid lines on the metal side. And all the electrons located at band tail states (short horizontal black lines) in the band gap of n^{++}-Si can tunnel through the barrier resulting in plasmons with energy as indicated by the vertical dotted blue arrow. The band tail states provide tunneling electrons at the energy less than the energy provided by the bias voltage. For the case of low doping concentration in n-Si as seen in Figure 5c and d, the emission comes mainly from the phonon-assisted indirect radiative recombination between electrons in the accumulation layer and holes in the valence band at the n-Si surface [43, 44]. Thus, the emission energy does not change with voltage bias, which is confirmed by the fixed value of the peaks (λ = 1100 nm) in sample (c). The blue-shift effect in the light emission spectra originating from surface-plasmon excitation via band tail states tunneling in Au/SiO_2/n^{++}-Si junction with a high doping concentration ($N_d \geq 10^{18}$ cm^{-3}), are reflected in Figure 5a and b. However, the light emissions coming from the MIS junctions with a low doping level (below 10^{18} cm^{-3}) is due to phonon-assisted indirect band-to-band recombination, as indicated in the insets of Figure 5c and d. The weak emission from such recombination does not result in any shift in the peak of the spectra with voltage bias.

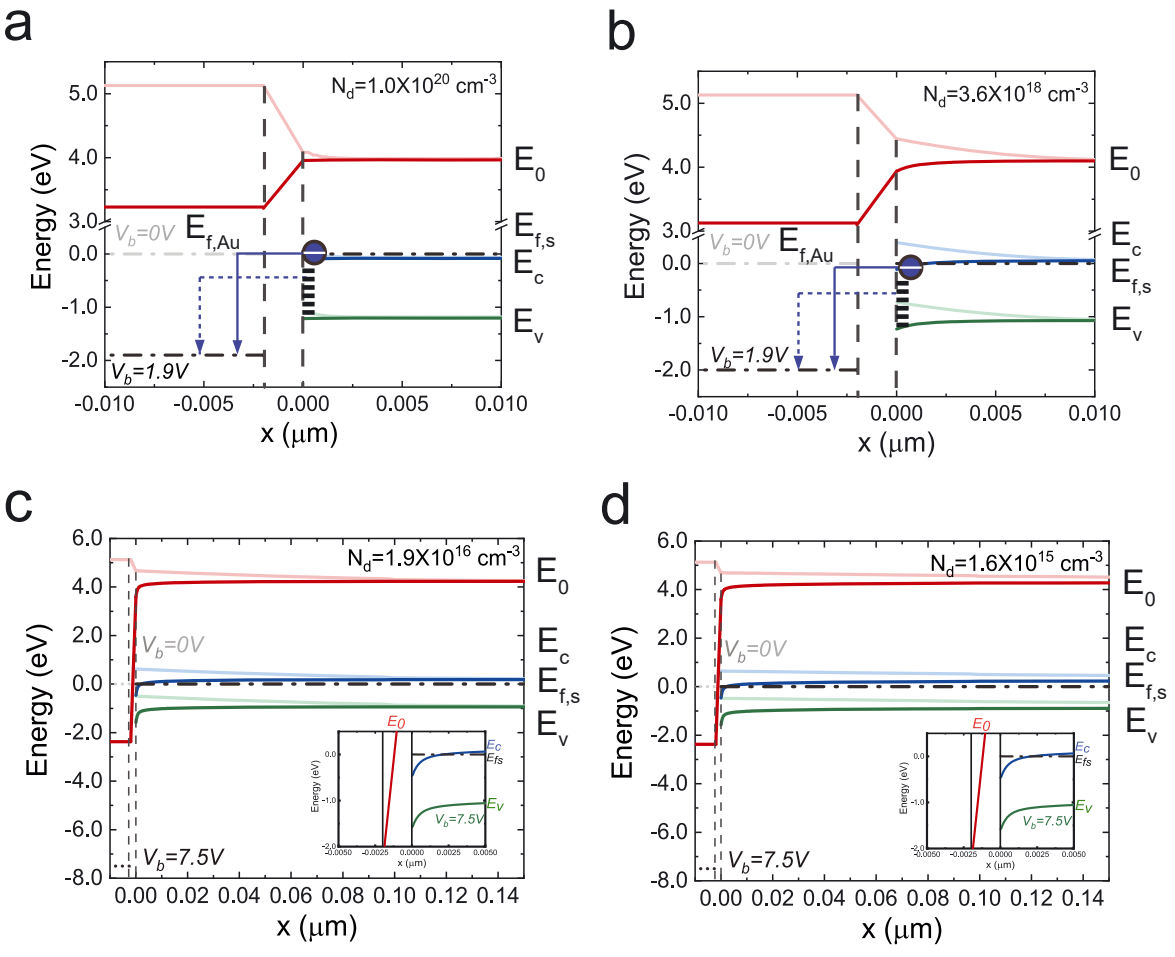

Figure 5: Energy band diagrams of Au/SiO_2/n-Si junctions at different voltage bias (faint line for the vacuum level is for V_b = 0, red line is for the higher voltage) (a) 1.0×10^{20} cm^{-3}, (b) 3.6×10^{18} cm^{-3}, (c) 1.9×10^{16} cm^{-3}, (d) 1.6×10^{15} cm^{-3} in n-Si. The insets of c and d are the zoom-in at the interface of SiO_2/n-Si.

4 Conclusions

In conclusion, we have theoretically demonstrated in this paper that surface plasmons can be excited at a low voltage bias by electron tunneling in an MIS structure Au/SiO_2/n^{++}-Si is attributed to the high density of band tail states in degenerated Si. The high density of band tail states in heavily doped Si (1.0×10^{20} cm^{-3}) aids the electron tunneling by lowering the barrier height, results in a lower voltage for tunneling and a larger tunneling current at a given voltage bias. Evidence of band tail states are obtained by C–V measurement. For samples with low doping concentration, there are no band tail states to help lower the tunneling barrier height. At a voltage bias of 2 V, the low doped samples give a tunneling current two orders of magnitude lower than that in the heavily doped sample. With low tunneling current at forward bias, phonon assisted indirect band-to-band recombination takes place between the accumulation layer in conduction band and valence band of n-Si. Therefore, the emitted light originating from the semiconductor is weak and the emitted wavelength does not shift with voltage bias being pegged to the bandgap energy of n-Si. This work paves the way for using MIS junction as a plasmonic actuator in integrated circuits. Given the small size of the plasmon actuator, it can be incorporated in front-end of line (FEOL). The electronic wires in Metal 1 layer can then be replaced with denser plasmonic waveguides thus squeezing more out of Moore's law.

Acknowledgments: We thank Prof Christian A. Nijhuis, Mr. Fangwei Wang (Ph. D student in Department of Chemistry), Dr. Lu Ding (IMRE, A-star), Dr. Dongyang Wan (Department of Physics, NUS) and Dr. Yu Cao (Department of ECE, NUS) who have kindly provided the constructive suggestions in devices fabrication and improvement.

Author contribution: Y. Liu conceived the experiments and simulations, analyzed the data, the organized the manuscript. S. P. Gao and W. R. Hu assisted in electrical characteristics, Y. X. Guo initiate the research and S. J. Chua verified the experimental data and simulation results and assisted in their interpretation and in the manuscript preparation.

Research funding: We acknowledge the support from the National Research Foundation Singapore project of Integration of Electrically Driven Plasmonic Components in High Speed (NRF-CRP17-2017-08).

Conflict of interest statement: The authors declare no conflicts of interest regarding this article.

References

[1] R. J. Martin-Palma and J. M. Martinez-Duart, *Nanotechnology for Microelectronics and Photonics*, 2nd ed., Kidlington, UK, Elsevier, 2017, ISBN 978-0-323-46176-4.

[2] W. Du, T. Wang, H.-S. Chu, and C. A. Nijhuis, "Highly efficient on-chip direct electronic–plasmonic transducers," *Nat. Photonics*, vol. 11, no. 10, pp. 623–627, 2017.

[3] H. Qian, S.-W. Hsu, K. Gurunatha, et al., "Efficient light generation from enhanced inelastic electron tunneling," *Nat. Photonics*, vol. 12, pp. 485–488, 2018.

[4] X. B. He, J. B. Tang, H. T. Hu, et al., "Electrically driven highly tunable cavity plasmons," *ACS Photonics*, vol. 6, no. 4, pp. 823–829, 2019.

[5] E. Ho-Seok, Y.-S. No, J. Kim, H.-G. Park, and M.-K. Seo, "Long-range surface plasmon polariton detection with a graphene photodetector," *Opt. Lett.*, vol. 43, no. 12, pp. 2889–2892, 2018.

[6] A. Masafumi, F. Yuriy, W. Heni, et al., "A high-speed, small-footprint plasmonic modulator is fabricated from a single layer of gold," *Science*, vol. 358, no. 6363, pp. 630–632, 2017.

[7] Y. Fang and M. Sun, "Nanoplasmonic waveguides: towards application in integration nanophotonic circuits," *Light Sci. Appl.*, vol. 4, no. e294, pp. 1–11, 2015.

[8] Y. Liu, L. Ding, Y. Cao, et al., "The deisgn of CMOS-compatible plasmonic waveguide for intra-chip communication," *IEEE Photonics J.*, vol. 12, no. 5, pp. 1–11, 2020, 4800810.

[9] K. Roy, B. Jung, D. Peroulis, and A. Raghunathan, "Integrated systems in the more-than-moore era: designing low-cost energy-efficient systems using heterogeneous components," *IEEE Des. Test*, vol. 33, no. 3, pp. 56–65, 2016.

[10] D. C. Tsui, "Observation of surface plasmon excitation by tunneling electrons in GaAs-Pd tunnel junctions," *Phys. Rev. Lett.*, vol. 22, no. 7, pp. 293–295, 1969.

[11] J. Watanabe, Y. Uehara, J. Murota, and S. Ushioda, "Light emission from Si-Metal-Oxide-Semiconductor tunnel junctions," *Jpn. J. Appl. Phys.*, vol. 32, no. 1A, pp. 99–104, 1993.

[12] M. X. Wang, J. H. Yu, and C. X. Sun, "Light emission characteristics and negative resistance phenomenon of Si-based metal/insulator/semiconductor tunnel junction," *Appl. Surf. Sci.*, vol. 161, pp. 9–13, 2000.

[13] H. Goktas, F. S. Gokhan, and V. J. Sorger, "Electrical-driven plasmon source of silicon based on quantum tunneling," *ACS Photonics*, vol. 5, no. 12, pp. 4928–4936, 2018.

[14] K. H. Gundlach, "Theory of metal-insulator-metal tunneling for a simple two-band model," *J. Appl. Phys.*, vol. 44, no. 11, pp. 5005–5010, 1973.

[15] G. T. Nicholas, *Metal-Insulator-Semiconductor Tunnel Junctions and Their Application to Photovoltaic Energy Conversion*, Ph. D Thesis, The University of British Columbia, 1981, pp. 64–98.

[16] F. Wang, Y. Liu, T. J. Duffin, et al., "A silicon-based quantum mechanical tunnel junction for plasmon excitation from low-energy tunneling electrons," *ACS Photonics*, vol. 8, no. 7, pp. 1951–1960, 2021.

[17] S. L. McCarthy and J. Lambe, "Enhancement of light emission from metal– insulator–metal tunnel junctions," *Appl. Phys. Lett.*, vol. 30, no. 8, pp. 427–429, 1977.

[18] K. S. Makarenko, T. J. D. Thanh Xuan Hoang, A. Radulescu, et al., "Efficient surface plasmon polariton excitation and control over outcoupling mechanism in metal-insulator-metal tunneling junctions," *Adv. Sci.*, vol. 7, no. 1900291, pp. 1–9, 2020.
[19] M. Parzefall, P. Bharadwaj, A. Jain, T. Taniguchi, K. Watanabe, and L. Novotny, "Antenna-coupled photon emission from hexagonal boron nitride tunnel junctions," *Nat. Nanotechnol.*, vol. 10, pp. 1058–1064, 2015.
[20] J. Lambe and S. L. McCarthy, "Light emission from inelastic electron tunneling," *Phys. Rev. Lett.*, vol. 37, pp. 923–925, 1976.
[21] P. Dawson, D. G. Walmsley, H. A. Quinn, and A. J. L. Ferguson, "Observation and explanation of light-emission spectra from statistically rough Cu, Ag, and Au tunnel junctions," *Phys. Rev. B*, vol. 30, pp. 3164–3178, 1984.
[22] J. Kirtley, T. N. Theis, and J. C. Tsang, "Light emission from tunnel junctions on gratings," *Phys. Rev. B*, vol. 24, pp. 5650–5663, 1981.
[23] M. Buret, A. V. Uskov, J. Dellinger, et al., "Spontaneous hot-electron light emission from electron-fed optical antennas," *Nano Lett*, vol. 15, pp. 5811–5818, 2015.
[24] W. E. Dahlke, "Tunneling into interface states of MOS structures," *Appl. Phys. Lett.*, vol. 10, no. 10, pp. 261–262, 1967.
[25] W. E. Dahlke and S. M. Sze, "Tunneling in metal-oxide-silicon structures," *Solid State Electron.*, vol. 10, no. 8, pp. 865–873, 1967.
[26] L. A. Kasprzak, "Dependence of the Si-SiO2 barrier height on SiO_2 thickness in MOS tunnel structure," *J. Appl. Phys.*, vol. 48, no. 10, pp. 4281–4286, 1977.
[27] S. Hlali, N. Hizem, and A. Kalboussi, "Investigation of capacitance characteristics in metal/high-k semiconductor devices at different parameters and with and without interface state density (traps)," *Bull. Mater. Sci.*, vol. 40, no. 5, pp. 1035–1041, 2017.
[28] H. Doğan, N. Yıldırım, İ. Orak, S. Elagöz, and A. Turut, "Capacitance-conductance-frequency characteristics of Au/Ni/n-GaN/undoped GaN Structures," *Phys. B Condens. Matter*, vol. 457, pp. 48–53, 2015.
[29] W. A. Harrison, "Tunneling from an independent-particle point of view," *Phys. Rev.*, vol. 123, no. 1, pp. 85–89, 1961.
[30] G. V. Naik, M. S. Vladimir, and A. Boltasseva, "Alternative plasmonic materials: beyond gold and silver," *Adv. Mater.*, vol. 25, pp. 3264–3294, 2013.
[31] D. Lu, J. J. Kan, E. E. Fullerton, and Z. Liu, "Enhancing spontaneous emission rates of molecules using nanopatterned multilayer hyperbolic metamaterials," *Nat. Nanotechnol.*, vol. 9, pp. 48–53, 2014.
[32] S. T. Chang, K. F. Chen, C. R. Shie, C. W. Liu, M.-J. Chen, and C.-F. Liu, "The band-edge light emission from the metal-oxide-silicon tunneling diode on (110) substrates," *Solid State Electron.*, vol. 46, pp. 1113–1116, 2002.
[33] I. V. Gekhov, A. F. Shulekin, and M. I. Vexler, "In tunnel MIS junction," in *MIEL conf. Proc*, 1997, pp. 165–168. 21st.
[34] C. W. Liu, M. H. Lee, C. F. Lin, W. T. Liu, and H. H. Liu, "Light emission and detection by metal oxide silicon tunneling diodes," *IEDM Conf. Proc.*, pp. 749–752, 1999.
[35] C. W. Liu, W. T. Liu, M. H. Lee, W. S. Kuo, and B. C. Hsu, "A novel photodetector using MOS tunneling structures," *IEEE Electron. Device Lett.*, vol. 21, no. 6, pp. 307–309, 2000.
[36] C. W. Liu, M. H. Lee, M.-J. Chen, I. C. Lin, and C.-F. Liu, "Room-temperature electroluminescence from electron-hole plasmas in the metal–oxide–silicon tunneling diodes," *Appl. Phys. Lett.*, vol. 76, no. 12, pp. 1516–1518, 2000.
[37] C. W. Liu, S. T. Chang, W. T. Liu, M.-J. Chen, and C.-F. Lin, "Hot carrier recombination model of visible electroluminescence from metal–oxide–silicon tunneling diodes," *Appl. Phys. Lett.*, vol. 77, no. 26, pp. 4347–4349, 2000.
[38] T. Matsuda, M. Nishio, T. Ohzone, and H. Hori, "Electroluminescence of MOS capacitors with Si-implanted SiO_2," *Solid-State Electron.*, vol. 41, no. 6, pp. 887–893, 1997.
[39] G. Z. Ran, J. S. Fu, W. C. Qin, B. R. Zhang, Y. P. Qiao, and G. G. Qin, "Blue to red electroluminescence from Au/native silicon oxide/p-Si structure subjected to rapid thermal annealing," *Thin Solid Films*, vol. 388, nos 1-2, pp. 213–216, 2001.
[40] J. Seidel, T. Gohler, S. Grafstrom, and L. M. Eng, "Near-field optical characterization of surface-plasmon-mediated light emission from electrically biased metal-insulator-semiconductor tunnel junctions," *Appl. Phys. Lett.*, vol. 92, no. 103123, pp. 1–3, 2008.
[41] M. X. Wang, J. H. Yu, and C. X Sun, "Light emission characteristics and negative resistance phenomenon of Si-based metal/insulator/semiconductor tunnel junction," *Appl. Surf. Sci.*, vol. 161, nos 1–2, pp. 9–13, 2000.
[42] M. Parzefall and L. Novotny, "Light at the end of tunnel," *ACS Photonics*, vol. 5, no. 11, pp. 4195–4202, 2018.
[43] S. Imhof and A. Thranhardt, "Phonon-assisted transitions and optical gain in indirect semiconductors," *Phys. Rev. B*, vol. 82, no. 085303, pp. 1–6, 2010.
[44] L. Pavesi, "Routes toward silicon-based lasers," *Mater. Today*, vol. 8, no. 1, pp. 18–25, 2005.

Supplementary Material: The online version of this article offers supplementary material (https://doi.org/10.1515/nanoph-2021-0287).